

Improved linear and Kerr nonlinear phase estimation via photon addition operations

Zekun Zhao¹, Qingqian Kang^{1,2}, Shoukang Chang³, Teng Zhao¹, Cunjin Liu¹, Xin Su¹, and Liyun Hu^{1,4*}

¹Center for Quantum Science and Technology, Jiangxi Normal University, Nanchang 330022, China

²Department of Physics, Jiangxi Normal University Science and Technology College, Nanchang 330022, China

³MOE Key Laboratory for Nonequilibrium Synthesis and Modulation of Condensed Matter,

Shaanxi Province Key Laboratory of Quantum Information and Quantum Optoelectronic Devices,

School of Physics, Xi'an Jiaotong University, Xi'an 710049, People's Republic of China

⁴Institute for Military-Civilian Integration of Jiangxi Province, Nanchang 330200, China

The accuracy of quantum measurements can be effectively improved by using both photon-added non-Gaussian operations and Kerr nonlinear phase shifters. Here, we employ coherent state mixed photon-added squeezed vacuum state as input into a Mach-Zehnder interferometer with parity detection, thereby achieving a significant enhancement in phase measurement accuracy. Our research focuses on phase sensitivity of linear phase shift under both ideal conditions and photon loss, as well as quantum Fisher information. The results demonstrate that employing the photon addition operations can markedly enhance phase sensitivity and quantum Fisher information, and the measurement accuracy can even approach the Heisenberg limit. In addition, we delve deeper into the scenario of replacing the linear phase shifter with a Kerr nonlinear one and systematically analyze the quantum Fisher information under both ideal and photon loss conditions. By comparison, it is evident that employing both the photon addition operations and the Kerr nonlinear phase shifter can further significantly enhance phase measurement accuracy while effectively improving the system's robustness against photon loss. These findings are instrumental in facilitating the development and practical application of quantum metrology.

PACS: 03.67.-a, 05.30.-d, 42.50.Dv, 03.65.Wj

I. INTRODUCTION

Quantum metrology leverages the non-classical characteristics of quantum states to achieve high-precision measurements, with broad applications in various fields of science and technology [1–6]. According to the principles of quantum mechanics, it is theoretically possible to surpass the accuracy limit set by classical physics, known as the standard quantum limit (SQL). This limit is represented by $1/\sqrt{\bar{N}}$, where \bar{N} is the total average photon number in the quantum state input to the system to be measured [7–9]. In the early 1980s, Caves introduced a coherent state (CS) and a squeezed vacuum state (SVS) into the two input ports of the Mach-Zehnder interferometer (MZI), enabling the measurement accuracy to surpass the SQL due to the non-classical properties of the input quantum states [9].

The non-classical characteristics of quantum states, particularly entanglement, have been identified as valuable resources for quantum technologies such as quantum communication [10, 11], quantum key distribution [12–14], and quantum metrology [15–21]. In quantum metrology, widely used interferometers comprise the linear MZI and the nonlinear SU(1,1) interferometer [22]. Numerous quantum states, such as NOON states [15–18] and entangled CSs [19–21], can be used as inputs to these interferometers, enhancing measurement accuracy beyond the SQL and potentially surpassing the Heisenberg limit (HL) of $1/\bar{N}$ [23]. However, these states are

not only more challenging to prepare but also exhibit heightened sensitivity to noise. For instance, while theoretically, highly entangled NOON states as inputs can achieve measurement accuracies up to the HL, experimental preparation is difficult and unstable [18, 24–27]. Thus, the preparation of non-classical quantum states, along with their robust anti-noise capabilities and stable transmission properties, holds significant importance in the field of quantum metrology. Recently, significant attention has been paid to the preparation of quantum states via non-Gaussian operations and their applications in quantum precision measurements. It has been demonstrated that non-Gaussian operations such as photon subtraction, photon addition, and photon catalysis effectively enhance non-classicality [28, 29], thereby improving measurement accuracy [30–38]. For example, Wang *et al.* proposed utilizing CS combined with photon-added SVS (PASVS) as inputs for lossless MZI to enhance measurement accuracy and compared it with CS mixed with photon-subtracted SVS (PSSVS) inputs. The results suggest that, under ideal conditions, photon addition and subtraction significantly enhance the phase sensitivity of parity detection. Notably, photon addition offers superior advantages in increasing phase measurement precision [38].

To improve measurement accuracy more effectively, replacing a linear phase shifter with a nonlinear one in conventional interferometers has gained increasing interest. Boixo *et al.* demonstrated that when employing entangled and product states as inputs to k th-order nonlinear Hamiltonians, the limits of phase sensitivity can reach \bar{N}^{-k} and $\bar{N}^{-(k-1/2)}$ respectively [39, 40]. In addition, recent studies have suggested schemes to improve

*hlyun@jxnu.edu.cn

the precision using a Kerr nonlinear phase shifter, showing that such approaches can surpass the HL [21, 41–47]. For example, Zhang *et al.* proposed enhancing the precision in an MZI by replacing the linear phase shifter with a Kerr nonlinear one, and used CS as the input state and parity detection. The results indicated that the parity detection signal offers high super-resolution for Kerr nonlinear phase shift, and the phase sensitivity effectively surpasses the HL, and approaches quantum Cramér-Rao bound (QCRB) [47]. However, the approach of employing both non-Gaussian operations and Kerr nonlinear phase shifter to improve phase estimation remains in the exploratory stage. Furthermore, photon loss unavoidably impacts measurement accuracy in practical applications, and there is a significant lack of systematic research addressing photon loss in this context.

Inspired by previous studies, this paper proposes the scheme of using CS and PASVS inputs to MZI and employing parity detection to achieve an effective improvement in the measurement accuracy. By examining the phase sensitivity and the quantum Fisher information (QFI) in both ideal and photon loss scenarios, it is evident that the non-Gaussian operations of photon addition significantly enhance the phase sensitivity and QFI. By increasing in the addition photon number, the phase sensitivity and QCRB can be significantly improved and can effectively outperform SQL and even approach HL. Furthermore, by considering the effects of photon loss, it can be found that the photon addition operations can effectively enhance the robustness of the system. We further replace the linear phase shifter with a Kerr nonlinear one in the MZI and investigate the QFI. By comparing the linear phase shift (under ideal conditions and photon loss), it is evident that the utilization of Kerr nonlinear phase shifter combined with photon addition can substantially enhance the QCRB. Moreover, the QCRB not only surpasses the sub-Heisenberg limit (sub-HL) of $1/\bar{N}^{3/2}$, but also potentially reaches the super-Heisenberg limit (SHL) of $1/\bar{N}^2$.

This paper is structured as follows: In Section II, we propose a phase estimation model that utilizes a combination of CS and PASVS as the input state for the MZI, incorporates parity detection at the output, and accounts for photon loss. Section III delves into the phase sensitivity in both the ideal case and the photon loss case. Section IV focuses on QFI including the effects of photon loss. Section V further explores the scheme of improving QFI and QCRB using Kerr nonlinear phase shift. Lastly, a summary is presented in the concluding section.

II. PHASE ESTIMATION MODEL FOR CS MIXED PASVS INPUT MZI

This section first introduces the phase estimation model based on MZI with CS and PASVS as the input states. As illustrated in Fig. 1, the balanced MZI includes

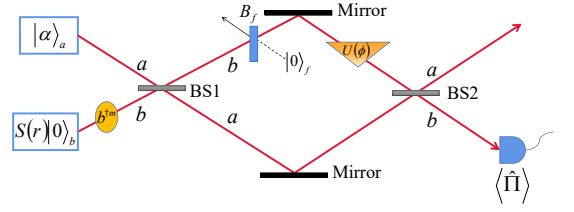


FIG. 1: Schematic diagram of phase estimation using CS and PASVS inputs in an MZI. In this configuration, photon loss within the MZI is simulated by a virtual beam splitter, and a parity detection scheme is employed at the output port.

two 50:50 optical beam splitters (BS1 and BS2) and a phase shifter. Based on the research by Yurke *et al.* [22], using angular momentum operators in the Schwinger representation, the equivalent operators for BS1 and BS2 are represented as $B_1 = \exp[-i\pi(a^\dagger b + ab^\dagger)/4]$ and $B_2 = \exp[i\pi(a^\dagger b + ab^\dagger)/4]$, respectively. These operators satisfy the transformation relations

$$B_1^\dagger \begin{pmatrix} a \\ b \end{pmatrix} B_1 = \frac{\sqrt{2}}{2} \begin{pmatrix} 1 & -i \\ -i & 1 \end{pmatrix} \begin{pmatrix} a \\ b \end{pmatrix}, \quad (1)$$

and

$$B_2^\dagger \begin{pmatrix} a \\ b \end{pmatrix} B_2 = \frac{\sqrt{2}}{2} \begin{pmatrix} 1 & i \\ i & 1 \end{pmatrix} \begin{pmatrix} a \\ b \end{pmatrix}. \quad (2)$$

The phase shifter operator is expressed as $U(\phi) = \exp[i\phi(b^\dagger b)]$, and the associated transformation relation is $U^\dagger(\phi)bU(\phi) = e^{i\phi}b$.

Our scheme aims to enhance the precision of phase measurement by utilizing CS and PASVS as input to the MZI. The input state is expressed as $|\psi\rangle_{in} = |\alpha\rangle_a \otimes |r, m\rangle_b$, where $|\alpha\rangle_a$ represents the CS at the a -mode input, and $|r, m\rangle_b$ denotes the PASVS at the b -mode input. The CS satisfies $a|\alpha\rangle_a = \alpha|\alpha\rangle_a$, where the amplitude parameter $\alpha = |\alpha|e^{i\theta}$. To simplify, we set $\theta = 0$ ($\alpha = |\alpha|$), making it more advantageous for enhanced phase estimation [38, 48]. The state $|r, m\rangle_b$ is generated through non-Gaussian operations involving m th-order photon addition $b^{\dagger m}$ to the SVS, defined as

$$|r, m\rangle_b = \frac{1}{\sqrt{P_m}} b^{\dagger m} S(r) |0\rangle_b, \quad (3)$$

where P_m represents the normalization factor, and $S(r) = \exp[r(b^2 - b^{\dagger 2})/2]$ denotes the squeezing operator with the squeezing parameter r . In particular, when $m = 0$, this corresponds to the scenario where CS mixed with SVS is utilized as input. For computational ease, we utilize $S(r)|0\rangle_b = \text{sech}^{1/2} r \exp[-b^{\dagger 2} \tanh r/2] |0\rangle_b$ and $b^{\dagger m} = \left. \frac{\partial^m}{\partial \tau^m} e^{b^\dagger \tau} \right|_{\tau=0}$. This representation leads to another expression of $|r, m\rangle_b$ as

$$|r, m\rangle_b = \frac{\frac{\partial^m}{\partial \tau^m} \exp[b^\dagger \tau - \frac{1}{2} b^{\dagger 2} \tanh r]}{\sqrt{P_m} \cosh r} \Big|_{\tau=0} |0\rangle_b, \quad (4)$$

thus, P_m and \bar{n}_b can be derived as

$$P_m = \frac{\partial^{2m}}{\partial t^m \partial \tau^m} e^{-\frac{\sinh 2r}{4}(t^2 + \tau^2)} e^{t\tau \cosh^2 r} \Big|_{t=\tau=0}, \quad (5)$$

$$\bar{n}_b = {}_b \langle r, m | b^\dagger b | r, m \rangle_b = \frac{P_{m+1}}{P_m} - 1. \quad (6)$$

In our scheme, the total average photon number $\bar{N} = {}_{in} \langle \psi | (a^\dagger a + b^\dagger b) | \psi \rangle_{in} = \bar{n}_a + \bar{n}_b$ with $\bar{n}_a = \alpha^2$.

Several studies have demonstrated that for specific path-symmetric state inputs to the MZI, parity detection using photon-number-resolving detectors can achieve the phase sensitivity saturating the QCRB. In this case, parity detection constitutes an optimal measurement scheme, leading to significant theoretical and experimental advancements [32–38, 45, 47–52, 60]. In the model illustrated in Fig. 1, parity detection is employed to measure the phase shift at the b -mode output port of the MZI, where the parity operator is defined as $\Pi_b = (-1)^{b^\dagger b} = e^{i\pi b^\dagger b}$.

To investigate the actual measurements, we simulated photon loss in the b -mode of the MZI by introducing a virtual beam splitter between BS1 and the phase shifter. The corresponding transformation relation is

$$B_f^\dagger \begin{pmatrix} b \\ b_f \end{pmatrix} B_f = \begin{pmatrix} \sqrt{1-l} & \sqrt{l} \\ -\sqrt{l} & \sqrt{1-l} \end{pmatrix} \begin{pmatrix} b \\ b_f \end{pmatrix}, \quad (7)$$

where b_f is the photon annihilation operator of the dissipative mode in which the vacuum noise $|0\rangle_f$ is located, and B_f represents the equivalent operator of a virtual beam splitter with reflectivity corresponding to a photon loss rate l . Specifically, $l = 0$ and $l = 1$ correspond to a lossless scenario and complete absorption, respectively.

To simplify the study of the parity detection scheme, we define an equivalent operator for parity detection that encompasses the entire lossy MZI, denoted as Π_b^{loss} , as follows:

$$\Pi_b^{loss} = {}_f \langle 0 | B_1^\dagger B_f^\dagger U^\dagger(\phi) B_2^\dagger \Pi_b B_2 U(\phi) B_f B_1 | 0 \rangle_f. \quad (8)$$

Using the normal ordering form of Π_b^{loss} , it is convenient to compute its average value with respect to the input state, i.e., $\langle \Pi_b \rangle = {}_{in} \langle \psi | \Pi_b^{loss} | \psi \rangle_{in}$. The value $\langle \Pi_b \rangle$ characterizes the signals of parity detection. The derivation procedure and specific expressions for the normal ordering form of Π_b^{loss} , as well as its average value $\langle \Pi_b \rangle$, are provided in Appendix A.

Using Eq. (A11) for the average value $\langle \Pi_b \rangle$, we can graph its behavior as a function of the phase shift ϕ . Fig. 2 illustrates $\langle \Pi_b \rangle$ with ϕ for both the ideal ($l = 0$) and photon loss ($l = 0.1$) cases. In Fig. 2(a), with fixed $\alpha = 2$ and $r = 0.5$, it is clearly demonstrated that the central peak or trough of $\langle \Pi_b \rangle$ at $\phi = 0$ narrows as the addition photon number m increases. This indicates that increasing m can effectively enhance the phase resolution of the parity signal. In addition, as shown in Fig. 2(b), when

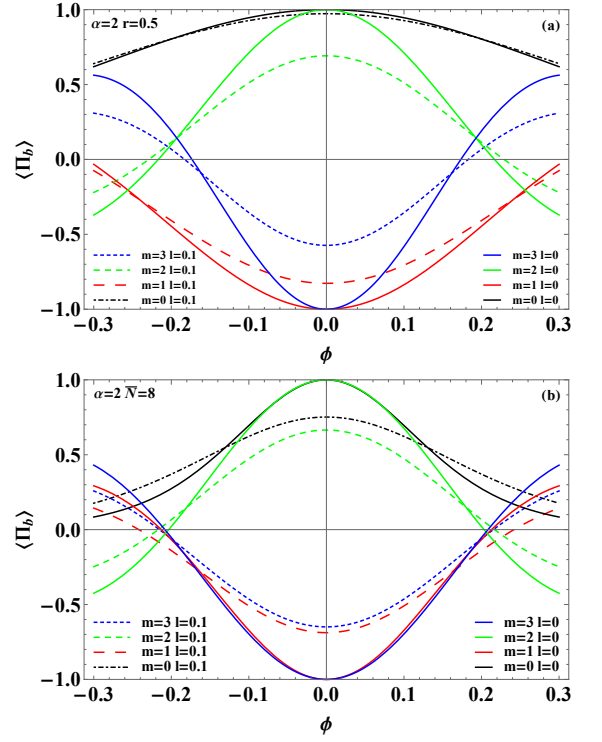


FIG. 2: The variation of the parity signal $\langle \Pi_b \rangle$ with phase shift ϕ for the ideal case ($l = 0$) and the photon loss case ($l = 0.1$), the addition photon number $m = 0, 1, 2, 3$ and the coherent amplitude $\alpha = 2$, (a) with the fixed squeezing parameter $r = 0.5$, and (b) with the fixed total average photon number $\bar{N} = 8$.

$\alpha = 2$ and $\bar{N} = 8$, the distribution of the central peak or trough remains largely consistent across different m due to the energy constraint imposed by the fixed the total average photon number \bar{N} . Furthermore, as illustrated in Fig. 2, photon loss results in a broader central peak or trough of $\langle \Pi_b \rangle$ relative to the ideal scenario. This shows that photon loss degrades the phase resolution. Based on the comparison of the dashed lines representing photon loss in Fig. 2(a), it is evident that the central peak or trough narrows as m increases. Thus, even in the presence of photon loss, phase resolution can be enhanced by photon addition operations, which implies that photon addition may improve the phase sensitivity of parity detection.

III. PHASE SENSITIVITY WITH PARITY DETECTION

For our scheme, the classical Fisher information (CFI) F_C for the phase shift ϕ can be obtained by using parity detection at the output port of the b -mode for even or odd photon numbers, as follows [49]:

$$F_C = \frac{1}{P_e} \left(\frac{\partial P_e}{\partial \phi} \right)^2 + \frac{1}{P_o} \left(\frac{\partial P_o}{\partial \phi} \right)^2, \quad (9)$$

where $P_e = (1 + \langle \Pi_b \rangle) / 2$ and $P_o = (1 - \langle \Pi_b \rangle) / 2$ represent the probabilities of even and odd counts, respectively. In this section, we investigate the phase sensitivity of parity detection, also referred to as phase uncertainty, under both ideal condition and photon loss. According to the Cramér-Rao bound, the error propagation formula for phase sensitivity can be derived using Eq. (9), i.e.,

$$\Delta\phi = \frac{1}{\sqrt{F_C}} = \frac{\sqrt{1 - \langle \Pi_b \rangle^2}}{|\partial \langle \Pi_b \rangle / \partial \phi|}. \quad (10)$$

By substituting Eq. (A11) into Eq. (10), one can derive the phase sensitivity $\Delta\phi$.

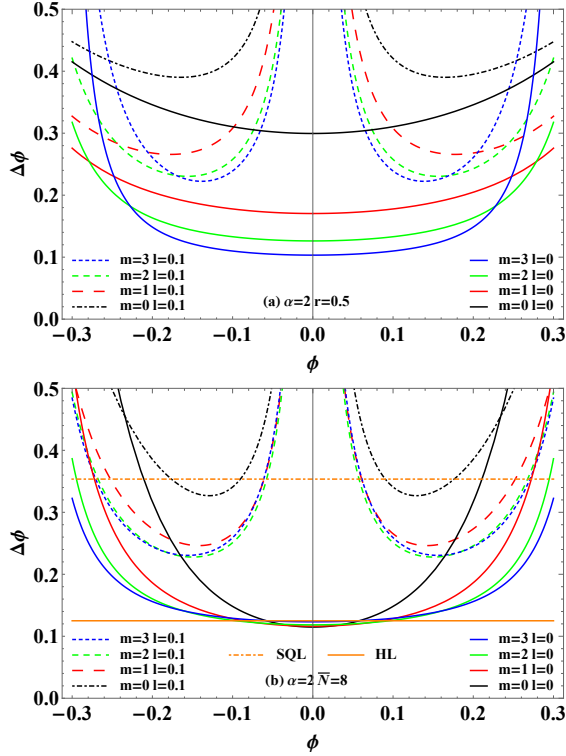


FIG. 3: For the addition photon number of $m = 0, 1, 2, 3$ and the coherent amplitude $\alpha = 2$, the phase sensitivity $\Delta\phi$ as a function of the phase shift ϕ for the ideal case ($l = 0$) and the photon loss case ($l = 0.1$), (a) with the fixed squeezing parameter $r = 0.5$, and (b) with the fixed total average photon number $\bar{N} = 8$ and compared with the SQL and the HL.

Fig. 3 illustrates the variation of the phase sensitivity $\Delta\phi$ with the phase shift ϕ for both the ideal ($l = 0$) and photon loss ($l = 0.1$) cases. As shown in the Fig. 3, in the ideal case, $\Delta\phi$ reaches its optimum when $\phi = 0$. Compared with the ideal scenario, photon loss degrades $\Delta\phi$ and causes the optimal point to deviate from $\phi = 0$. As depicted in Fig. 3(a), when $\alpha = 2$ and $r = 0.5$ are given, $\Delta\phi$ can be effectively enhanced by increasing the addition photon number m within a certain range near the optimal point of ϕ . Furthermore, according to Refs. [38, 48, 53, 54], $\Delta\phi$ yields favorable results when $\bar{n}_a = \bar{n}_b$ and \bar{N} is fixed at a suitably large value. Thus, to

further investigate the enhancement effect of our scheme on phase sensitivity $\Delta\phi$, Fig. 3(b) illustrates $\Delta\phi$ as a function of ϕ for $\alpha = 2$ and $\bar{N} = 8$ ($\bar{n}_a = \bar{n}_b = 4$), and compares it with the SQL and the HL. It is shown that the ideal $\Delta\phi$ significantly surpasses the SQL and approaches the HL near the optimal point $\phi = 0$. Moreover, near $\phi = 0$, $\Delta\phi$ remains essentially the same for $m = 0, 1, 2, 3$ due to the energy constraint imposed by the fixed \bar{N} , while $\Delta\phi$ improves with increasing m when ϕ deviates from 0 for a certain range. Compared with the ideal case, the photon loss with $l = 0.1$ makes the phase sensitivity $\Delta\phi$ deteriorate, and the optimal point deviates from $\phi = 0$. However, by using the photon addition operations of $m = 1, 2, 3$, $\Delta\phi$ can be significantly improved relative to $m = 0$, and $\Delta\phi$ can still effectively break through the SQL within a certain range.

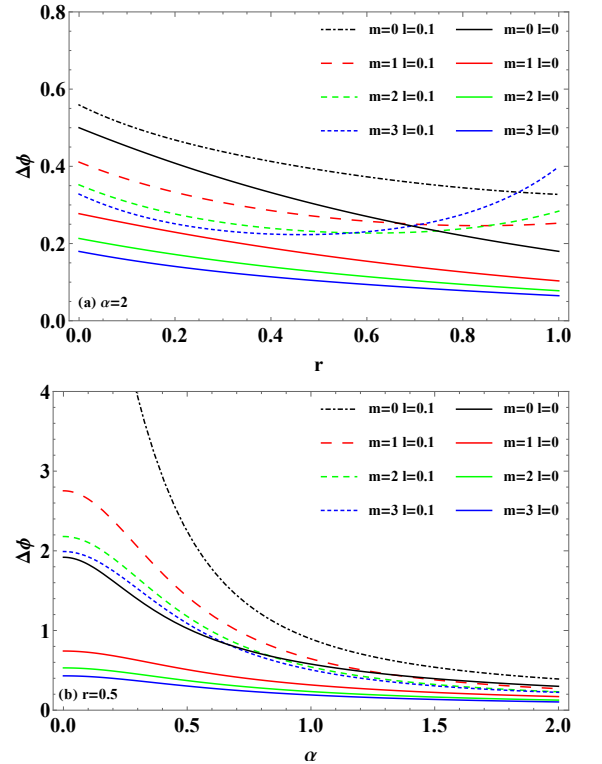


FIG. 4: In the ideal case ($l = 0$) with fixed the phase shift $\phi = 10^{-4}$ and the photon loss case ($l = 0.1$) with fixed $\phi = 0.15$, for the addition photon number $m = 0, 1, 2, 3$, (a) the phase sensitivity $\Delta\phi$ as a function of the squeezing parameter r with the coherent amplitude $\alpha = 2$, (b) $\Delta\phi$ as a function of α with $r = 0.5$.

As shown in Fig. 4, the phase sensitivity $\Delta\phi$ as a function of the squeezing parameter r and coherent amplitude α is depicted under both the ideal ($l = 0$) and photon loss ($l = 0.1$) scenarios. It is evident that the ideal $\Delta\phi$ can be enhanced by increasing r , α and the addition photon number m for a small phase shift $\phi = 10^{-4}$. Despite the impact of photon loss, when an appropriate $\phi = 0.15$ is selected (as illustrated in Fig. 3, photon loss results in the optimal ϕ point deviating from 0), $\Delta\phi$ can

still be significantly enhanced by increasing r , α and m within a certain range. Specifically, in Fig. 4(a), it is observed that under the photon loss, as m increases, the range over which $\Delta\phi$ improves with increasing r is confined to relatively small values of r . Actually, the smaller squeezing parameter r values are more experimentally feasible.

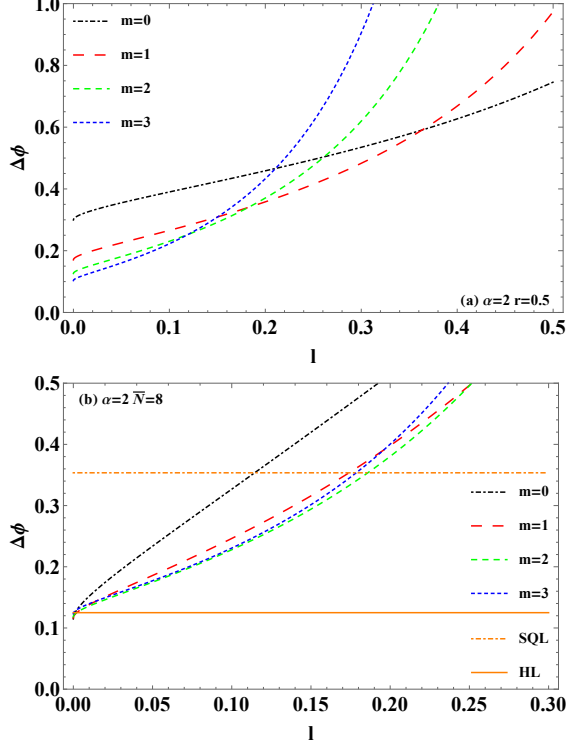


FIG. 5: For the addition photon number $m = 0, 1, 2, 3$, the coherent amplitude $\alpha = 2$, and optimized the phase shift ϕ , the phase sensitivity $\Delta\phi$ as a function of loss rate l (a) for given the squeezing parameter $r = 0.5$, and (b) for given the total average photon number $\bar{N} = 8$, and compared with the SQL and the HL.

To further analyze the influence of photon loss on phase sensitivity $\Delta\phi$, as shown in Fig. 5, we present the variation of $\Delta\phi$ with respect to the loss rate l (phase shift ϕ is optimized). Although $\Delta\phi$ deteriorates with the increase of the loss rate l (see Fig. 5(a)), when $\alpha = 2$ and $r = 0.5$ are fixed, $\Delta\phi$ can still be significantly improved by the photon addition operations of $m = 1, 2, 3$ within a certain range of relatively small l . Fig. 5(b) shows $\Delta\phi$ versus l for $\alpha = 2$ and $\bar{N} = 8$, comparing the SQL and HL. It can be found that $\Delta\phi$ can reach the HL when l is very small, and in the case of photon loss, $\Delta\phi$ can still effectively break through the SQL in a certain range of l . Compared to the case of $m = 0$, $\Delta\phi$ of $m = 1, 2, 3$ has a significant improvement and can exceed the SQL in a larger range of l . This indicates that the photon addition operations enhance the robustness of the measured system.

IV. THE QFI IN MZI

The QFI quantifies the maximum amount of obtainable information regarding the phase shift ϕ of a quantum system, independent of any detection scheme, and it is an upper bound of the CFI. The optimal error bound for phase sensitivity, known as the QCRB, is given by [55–57]

$$\Delta\phi_{QCRB} = \frac{1}{\sqrt{F_Q}}, \quad (11)$$

where F_Q is the QFI. For a pure state, the QFI under ideal condition can be calculated as [58]

$$F_Q = 4 \left[\langle \psi'_\phi | \psi'_\phi \rangle - |\langle \psi'_\phi | \psi_\phi \rangle|^2 \right], \quad (12)$$

where $|\psi_\phi\rangle = U(\phi) B_1 |\psi\rangle_{in}$ is the quantum state before BS2 in the lossless MZI, and $|\psi'_\phi\rangle = \partial |\psi_\phi\rangle / \partial \phi$. Thus, the QFI can be further simplified as

$$F_Q = 4 \langle \Delta^2 n_b \rangle = 4 \left[\langle n_b^2 \rangle - \langle n_b \rangle^2 \right], \quad (13)$$

where $n_b = b^\dagger b$, and $\langle \cdot \rangle = \langle \Psi_S | \cdot | \Psi_S \rangle$, with $|\Psi_S\rangle = B_1 |\psi\rangle_{in}$.

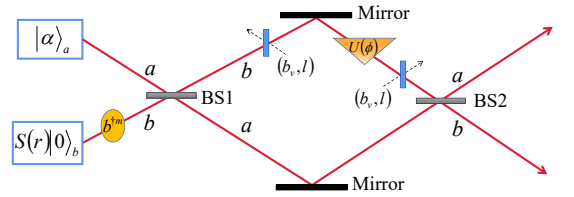


FIG. 6: Theoretical model of lossy MZI using CS mixed with PASVS as input. Two virtual optical beam splitters, positioned before and after the phase shifter, simulate photon loss. The parameter l represents the reflectivity, or loss rate, of the optical beam splitter, while b_v denotes the vacuum operator.

For the initial pure state $|\Psi_S\rangle$ in a probe system S with a lossy MZI, we introduce the orthogonal states $|j_E\rangle$ of the environment E and the Kraus operator $\hat{\Pi}_j(\phi)$ to characterize the behavior of $|\Psi_S\rangle$ as it passes through the phase shifter, accounting for photon loss. A diagram illustrating photon loss inside the MZI is provided in Fig. 6. According to Escher *et al.*'s methods for calculating QFI in open quantum systems [59], the quantum states of $|\Psi_S\rangle$ and the vacuum noise in the environment $|0_E\rangle$, after undergoing unitary evolution $U_{S+E}(\phi)$ that accounts for photon loss, can be expressed in the extended space of $S + E$ as

$$\begin{aligned} |\Psi_{S+E}\rangle &= U_{S+E}(\phi) |\Psi_S\rangle |0_E\rangle \\ &= \sum_{j=0}^{\infty} \hat{\Pi}_j(\phi) |\Psi_S\rangle |j_E\rangle. \end{aligned} \quad (14)$$

Indeed, after photon loss, the quantum state $|\Psi_S\rangle$ transitions into a mixed state; however, we employ this approach to treat the quantum state $|\Psi_{S+E}\rangle$ in $S + E$ as a pure state. In this context, for the entire purified system, the QFI under photon loss can be expressed as

$$F_Q \leq C_Q \left[|\Psi_S\rangle, \hat{\Pi}_j(\phi) \right] = 4 \left[\langle \hat{H}_1 \rangle - \left| \langle \hat{H}_2 \rangle \right|^2 \right], \quad (15)$$

where the lower bound of $C_Q \left[|\Psi_S\rangle, \hat{\Pi}_j(\phi) \right]$ is demonstrated to be the QFI for a reduced system [59], and $\hat{H}_{1,2}$ are Hermitian operators defined as

$$\hat{H}_1 = \sum_{j=0}^{\infty} \frac{d\hat{\Pi}_j^\dagger(\phi)}{d\phi} \frac{d\hat{\Pi}_j(\phi)}{d\phi}, \quad (16)$$

$$\hat{H}_2 = i \sum_{j=0}^{\infty} \frac{d\hat{\Pi}_j^\dagger(\phi)}{d\phi} \hat{\Pi}_j(\phi), \quad (17)$$

where $\hat{\Pi}_j(\phi)$ is the Kraus operator, i.e.,

$$\hat{\Pi}_j(\phi) = \sqrt{\frac{l^j}{j!}} e^{i\phi(b^\dagger b - \gamma j)} (1-l)^{\frac{b^\dagger b}{2}} b^j, \quad (18)$$

where $\gamma = 0$ or -1 correspond to photon loss before or after the linear phase shifter, respectively. By optimizing γ , we can derive $C_{Q\min}$. Thus, the QFI in the presence of photon loss is obtained as [59]

$$F_Q = \frac{4(1-l) \langle n_b \rangle \langle \Delta^2 n_b \rangle}{l \langle \Delta^2 n_b \rangle + (1-l) \langle n_b \rangle}, \quad (19)$$

where, $\langle n_b \rangle$ and $\langle n_b^2 \rangle$ can be obtained by setting w of $\langle n_b^w \rangle$ in Eq. (B3) to 1 and 2, respectively (see Appendix B for details).

Fig. 7 illustrates the variation of the QFI with respect to the input state parameters and the impact of photon loss ($l = 0.1$) on the QFI. It is clear that, although photon loss decreases the QFI F_Q , increasing the squeezing parameter r , the coherent amplitude α , and the addition photon number m can effectively increase F_Q , thereby improving the QCRB as indicated by Eq. (11) ($\Delta\phi_{QCRB} = 1/\sqrt{F_Q}$), in both the ideal and photon loss cases. Thus, the proposed input scheme can effectively improve the accuracy of phase measurement.

In order to investigate the effect of photon loss on the QCRB $\Delta\phi_{QCRB}$, we plot the variation of $\Delta\phi_{QCRB}$ with the loss rate l in Fig. 8. It can be found that $\Delta\phi_{QCRB}$ deteriorates gradually as l increases. As can be seen in Fig. 8(a), $\Delta\phi_{QCRB}$ can still be effectively improved by increasing m in the case of photon loss. This indicates that the robustness of the system to photon loss is significantly enhanced by using photon addition operations. In Fig. 8(b), it can be observed that $\Delta\phi_{QCRB}$ can effectively surpass the SQL and even exceed the HL within a

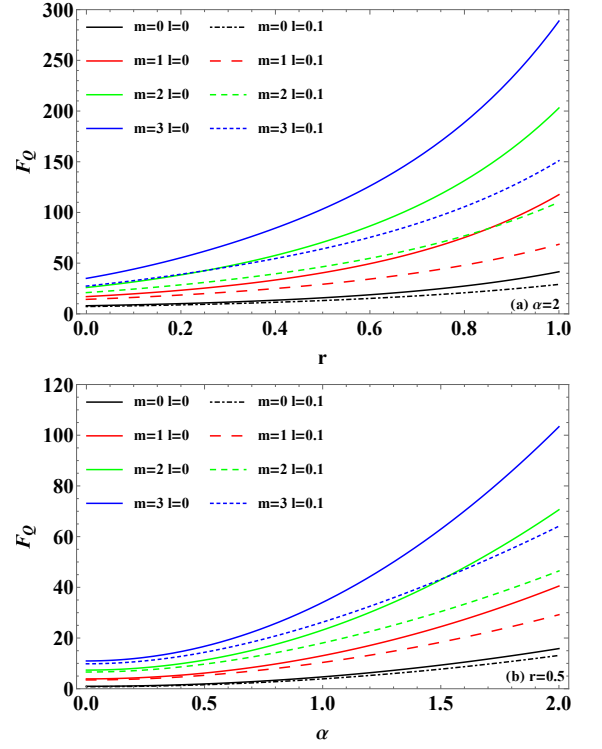


FIG. 7: For the addition photon number $m = 0, 1, 2, 3$, in the ideal case of $l = 0$, and in the photon loss case of $l = 0.1$, (a) the variation of QFI F_Q with the squeezing parameter r for given the coherent amplitude $\alpha = 2$, and (b) the variation of F_Q with α for given $r = 0.5$.

certain range of l , despite photon loss. Additionally, the $\Delta\phi_{QCRB}$ is essentially the same for different m since \bar{N} corresponding to the input resource energy is fixed.

As shown in Fig. 9, the variation of the QCRB $\Delta\phi_{QCRB}$ with respect to the total average photon number \bar{N} is demonstrated and compared to the phase sensitivity $\Delta\phi$ as well as to the SQL and the HL. It can be clearly seen that for both the ideal ($l = 0$) and photon loss ($l = 0.1$) cases, $\Delta\phi_{QCRB}$ and $\Delta\phi$ can be improved with the increase of \bar{N} and m when the fixed squeezing parameter $r = 0.5$. As illustrated in Fig. 9(a), under ideal condition, $\Delta\phi_{QCRB}$ and $\Delta\phi$ can evidently surpass the SQL and even approach the HL. Additionally, as m increases, $\Delta\phi$ progressively converges towards $\Delta\phi_{QCRB}$. Thus, in an ideal scenario, optimal measurement for CS mixed PASVS input MZI scheme can be achieved by employing parity detection. Fig. 9(b) illustrates that despite photon loss, $\Delta\phi_{QCRB}$ and $\Delta\phi$ can still effectively break through the SQL, and can be significantly improved by increasing \bar{N} and utilizing photon addition operations.

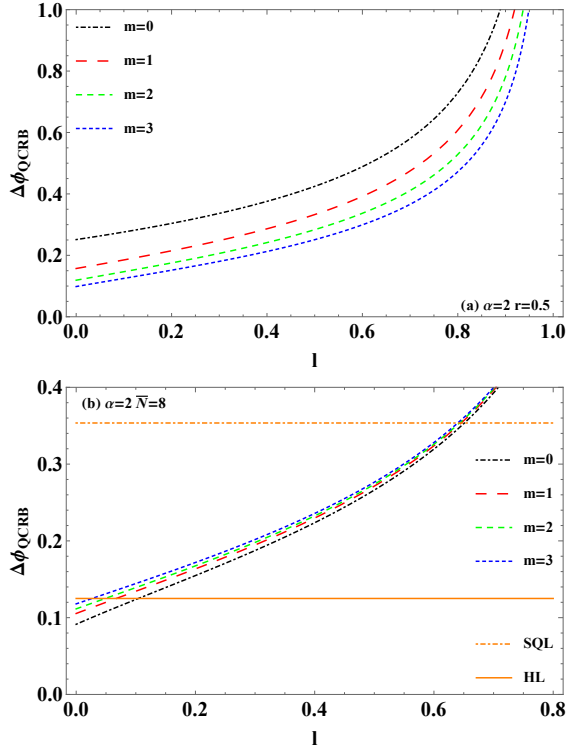


FIG. 8: For the addition photon number $m = 1, 2, 3$, and the coherent amplitude $\alpha = 2$, the QCRB $\Delta\phi_{QCRB}$ as a function of loss rate l , (a) for given the squeezing parameter $r = 0.5$, and (b) for given the total average photon number $\bar{N} = 8$, and compared with the SQL and the HL.

V. THE QFI IMPROVED BY KERR NONLINEAR PHASE SHIFTER

Theoretically, the Kerr nonlinear transformation can substantially enhance measurement accuracy compared to the phase encoding process using linear transformation. Thus, this section further investigates the QFI in the case of replacing the linear phase shifter $U(\phi)$ in the model of Fig. 6 with a Kerr nonlinear phase shifter $U_K(\phi)$. Building upon prior research methodologies for the QFI with linear phase shift under both ideal and photon loss conditions, we further investigate the QFI in the Kerr nonlinear phase shift case. The Kerr nonlinear phase shifter operator is defined as $U_K(\phi) = \exp[i\phi(b^\dagger b)^2]$, so according to Eq. (12) and substituting $|\psi_\phi\rangle = U_K(\phi)B_1|\psi\rangle_{in}$, the QFI for the Kerr nonlinear case under the ideal condition can be derived as

$$F_Q = 4 \langle \Delta^2 n_b^2 \rangle = 4 [\langle n_b^4 \rangle - \langle n_b^2 \rangle^2]. \quad (20)$$

Substituting $w = 2$ and $w = 4$ into Eq. (B3) to obtain $\langle n_b^2 \rangle$ and $\langle n_b^4 \rangle$, and further substituting them into Eq. (20), the QFI for the ideal case of Kerr nonlinear phase shift can be obtained.

Next, we investigate the QFI of photon loss for the Kerr nonlinear case. The general form of the Kraus operator,

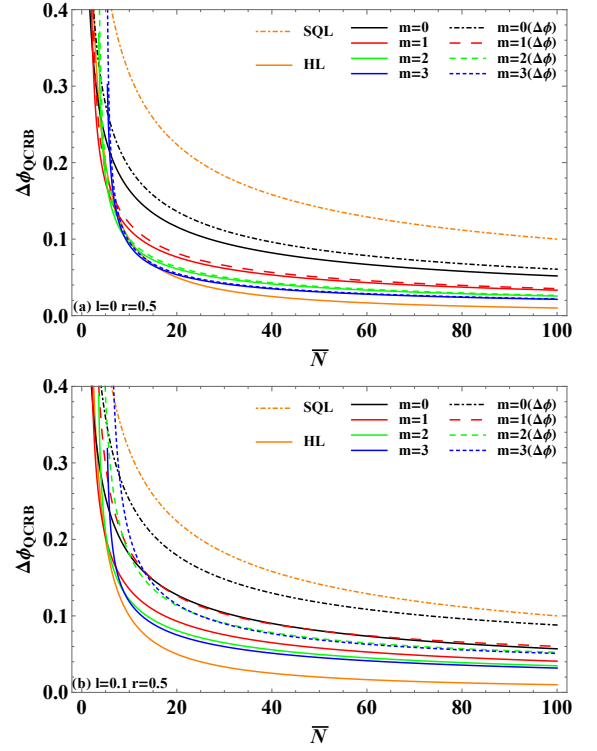


FIG. 9: The QCRB $\Delta\phi_{QCRB}$ as a function of the total average photon number \bar{N} for the addition photon number $m = 0, 1, 2, 3$, and fixed the squeezing parameter $r = 0.5$, (a) in the ideal case of $l = 0$, and (b) in the photon loss case of $l = 0.1$. The SQL, the HL and the variation of phase sensitivity $\Delta\phi$ with respect to \bar{N} (for $l = 0$ and $l = 0.1$, fixed the phase shift $\phi = 10^{-4}$ and optimization ϕ , respectively) are also plotted for comparison.

incorporating the Kerr nonlinear phase shift, is defined as follows [46]:

$$\hat{\Pi}_j(\phi) = \sqrt{\frac{l^j}{j!}} e^{i\phi[(b^\dagger b)^2 - 2\mu_1 b^\dagger b j - \mu_2 j^2]} (1-l)^{\frac{b^\dagger b}{2}} b^j, \quad (21)$$

where l is the loss rate, and the parameters $\mu_1 = \mu_2 = 0$ or -1 correspond to photon loss occurring before or after the Kerr nonlinear phase shifter. Referring to Eq. (15), we derive (see Appendix C for derivation):

$$\begin{aligned} F_Q &\leq C_Q [|\Psi_S\rangle, \hat{\Pi}_j(\phi)] \\ &= 4 [K_1^2 \langle \Delta^2 n_b^2 \rangle - K_2 \langle n_b^3 \rangle + K_3 \langle n_b^2 \rangle \\ &\quad - K_4 \langle n_b \rangle - K_5 \langle n_b^2 \rangle \langle n_b \rangle - K_6 \langle n_b \rangle^2], \quad (22) \end{aligned}$$

where K_i ($i = 1, 2, 3, 4, 5, 6$) are detailed in Appendix C. To determine the QFI F_Q under photon loss for the Kerr nonlinear case, substitute the optimal values of μ_1 and μ_2 (μ_{1opt} and μ_{2opt}) into C_Q to find C_{Qmin} . The specific expressions for μ_{1opt} and μ_{2opt} are provided in Appendix C.

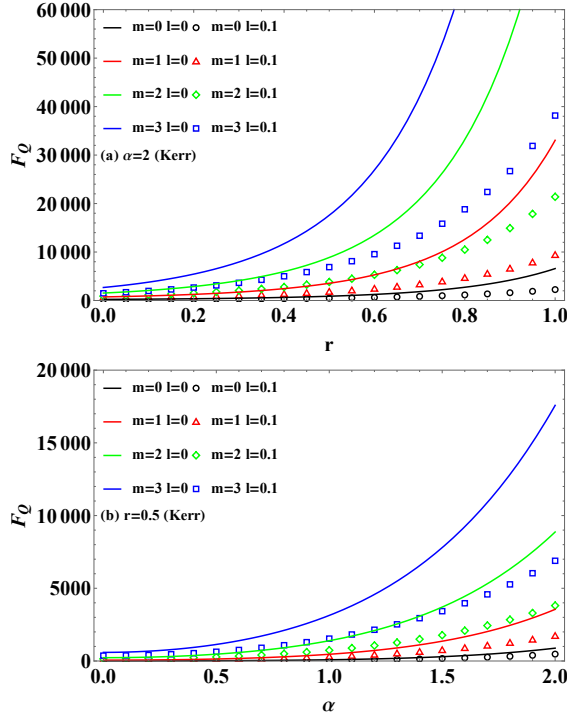


FIG. 10: For the Kerr nonlinear phase shift case, and the addition photon number $m = 0, 1, 2, 3$, in the ideal case of $l = 0$ and in the photon loss case of $l = 0.1$, (a) the variation of QFI F_Q with the squeezing parameter r for given the coherent amplitude $\alpha = 2$, and (b) the variation of F_Q with α for given $r = 0.5$.

Fig. 10 illustrates the QFI F_Q variation with the squeezing parameter r and coherent amplitude α for the Kerr nonlinear case, considering both ideal and photon loss scenarios. Clearly, F_Q increases with r , α , and the addition photon number m . A comparison between Fig. 7 and Fig. 10 indicates that the QFI exhibits a substantial increase in the case of Kerr nonlinear phase shift relative to the linear one. Hence, these results demonstrate that QFI and the phase measurement accuracy of QCRB can be effectively increased by enhancing input resources of r and α , utilizing photon addition operations, and the Kerr nonlinear phase shifter.

For the Kerr nonlinear case, the variation of QCRB $\Delta\phi_{QCRB}$ with loss rate l is shown in Fig. 11. By comparing Fig. 11(a) to Fig. 8(a), a similar conclusion can be obtained, i.e., although photon loss worsens $\Delta\phi_{QCRB}$, the use of the photon addition operations remains effective in improving $\Delta\phi_{QCRB}$, and $\Delta\phi_{QCRB}$ improves as m increases. $\Delta\phi_{QCRB}$ of Fig. 11 has a significant improvement with respect to the linear phase shift case of Fig. 8. Moreover, it can be found from Fig. 11(b) that $\Delta\phi_{QCRB}$ can break through the HL over a large range of l and can break through the sub-HL and even surpass the SHL over a certain range of l . This indicates that the utilization of the Kerr nonlinear phase shifter can significantly improve the QCRB and the robustness of the system to

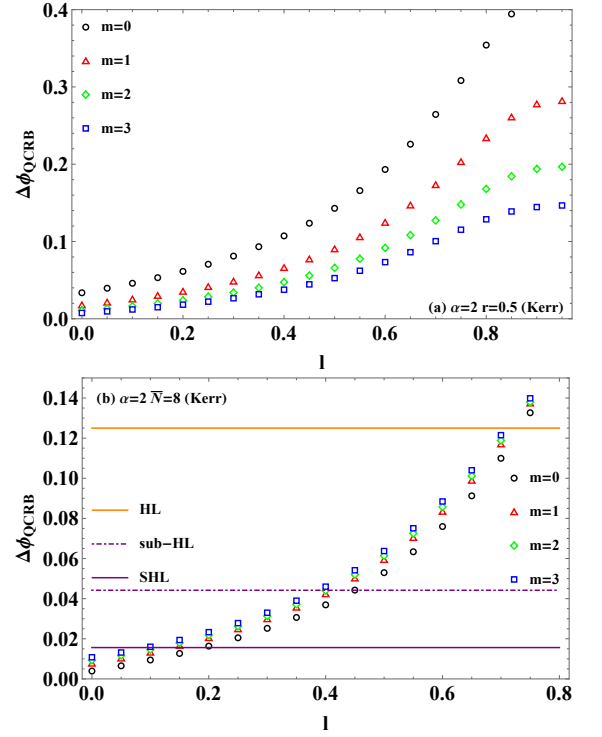


FIG. 11: For the Kerr nonlinear phase shift case, the addition photon number $m = 1, 2, 3$, and the coherent amplitude $\alpha = 2$, the QCRB $\Delta\phi_{QCRB}$ as a function of loss rate l , (a) for given the squeezing parameter $r = 0.5$, and (b) for given the total average photon number $\bar{N} = 8$, and compared with the SQL and the HL.

photon loss.

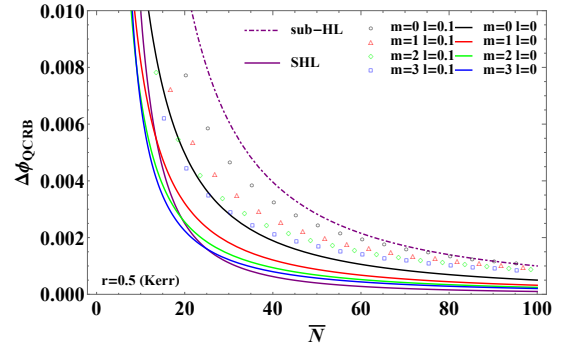


FIG. 12: For the Kerr nonlinear phase shift case, the addition photon number $m = 0, 1, 2, 3$, and fixed the squeezing parameter $r = 0.5$, in the ideal case of $l = 0$ and in the photon loss case of $l = 0.1$, the variation of QCRB $\Delta\phi_{QCRB}$ with respect to the total average photon number \bar{N} . The HL, sub-HL, and SHL are also plotted for comparison.

To further reflect the improved effect of the Kerr nonlinear phase shift on the accuracy, Fig. 12 depicts the variation of the QCRB $\Delta\phi_{QCRB}$ with respect to the total average photon number \bar{N} and compares it with the HL, sub-HL, and SHL. It is clear from the images that

$\Delta\phi_{QCRB}$ can be effectively improved for both the ideal ($l = 0$) and photon loss ($l = 0.1$) cases by increasing \bar{N} and m . Furthermore, in the ideal case, $\Delta\phi_{QCRB}$ of the Kerr nonlinear phase shift can break through the sub-HL to a large extent, and the photon addition operations of $m = 1, 2, 3$ can make $\Delta\phi_{QCRB}$ approach or even exceed the SHL. In the case of $l = 0.1$, $\Delta\phi_{QCRB}$ improved by the photon addition operations can still effectively break through the sub-HL. Thus, the utilization of both the photon addition operations and the Kerr nonlinear phase shifter can significantly improve the measurement accuracy.

VI. CONCLUSION

We propose a scheme that utilizes CS and PASVS inputs in an MZI to improve the precision of phase measurements. Our primary focus is on investigating the phase sensitivity of parity detection and the QFI, both under ideal conditions and in the presence of photon loss. The results indicate that phase measurement accuracy is significantly improved by optimizing input resources, i.e. increasing the squeezing parameter r , coherent amplitude α , and total average photon number \bar{N} . Furthermore, the comparison reveals that the non-Gaussian operations of photon addition markedly enhance phase sensitivity and QFI. In the ideal case, the phase sensitivity and QCRB improve with increasing the addition photon number m , significantly surpassing the SQL and even reaching the HL. In addition, the phase sensitivity can be better approximated to the QCRB by increasing m , which indicates that the parity detection is an optimal measurement for the phase estimation of the CS mixed PASVS inputs MZI. In the presence of photon loss, phase sensitivity and QCRB can still be significantly enhanced by increasing m , allowing the SQL to be surpassed across a relatively broad range of loss rates l .

In order to achieve a more effective improvement in measurement accuracy using the CS mixed PASVS input scheme, we further considered replacing the linear phase shifter of MZI with a Kerr nonlinear phase shifter. Based on the study of QFI for the Kerr nonlinear phase shift scenario, it is evident that both QFI and QCRB can be substantially enhanced in both the ideal case and the photon loss case by increasing the parameters r , α , and \bar{N} , as well as optimizing the photon addition operation through an increase in m . Comparing the linear phase shift case, it can be clearly found that the Kerr nonlinear phase shift has a significant improvement on the QFI and QCRB, and the QCRB at photon loss can break through the HL over a wide range of the loss rate l , and can effectively exceed the sub-HL and even surpass the SHL over a certain range. Our findings demonstrate that employing photon addition operations and Kerr nonlinear phase shifter effectively enhances phase measurement accuracy and robustness to photon loss in practical applications. This research is pivotal for advancing quantum precision

measurement.

Acknowledgments

This work is supported by the National Natural Science Foundation of China (Grants No. 11964013 and No. 12104195) and the Jiangxi Provincial Natural Science Foundation (Grants No. 20242BAB26009 and 20232BAB211033), Jiangxi Provincial Key Laboratory of Advanced Electronic Materials and Devices (Grant No. 2024SSY03011), Jiangxi Civil-Military Integration Research Institute (Grant No. 2024JXRH0Y07), as well as the Science and Technology Project of Jiangxi Provincial Department of Science and Technology (Grant No. GJJ2404102).

APPENDIX A : THE NORMAL ORDERING OF PARITY OPERATOR AND ITS AVERAGE VALUE

To facilitate the computation of the normal ordering form of the equivalent operator for parity detection Π_b^{loss} encompassing the entire lossy MZI, we first present the Weyl ordering form representation of the parity operator Π_b in the ideal case [60, 61], as follows

$$\Pi_b = \frac{\pi}{2} \begin{smallmatrix} \vdots \\ \bullet \\ \vdots \end{smallmatrix} \delta(b) \delta(b^\dagger) \begin{smallmatrix} \vdots \\ \bullet \\ \vdots \end{smallmatrix}, \quad (A1)$$

where $\begin{smallmatrix} \vdots \\ \bullet \\ \vdots \end{smallmatrix}$ is the Weyl ordering and $\delta(\cdot)$ denotes the delta function. According to Eq. (8), by employing the invariance of Weyl ordering under similarity transformations [62] and combining the linear phase shift case with the operator transformation relation concerning the lossy MZI, we obtain

$$\begin{aligned} \Pi_b^{loss} &= {}_f \langle 0 | U_{MZI}^\dagger \Pi_b U_{MZI} | 0 \rangle_f \\ &= \frac{\pi}{2} {}_f \langle 0 | U_{MZI}^\dagger \begin{smallmatrix} \vdots \\ \bullet \\ \vdots \end{smallmatrix} \delta(b) \delta(b^\dagger) \begin{smallmatrix} \vdots \\ \bullet \\ \vdots \end{smallmatrix} U_{MZI} | 0 \rangle_f \\ &= \frac{\pi}{2} {}_f \langle 0 | \begin{smallmatrix} \vdots \\ \bullet \\ \vdots \end{smallmatrix} U_{MZI}^\dagger \delta(b) \delta(b^\dagger) U_{MZI} \begin{smallmatrix} \vdots \\ \bullet \\ \vdots \end{smallmatrix} | 0 \rangle_f, \end{aligned} \quad (A2)$$

where $U_{MZI} = B_2 U(\phi) B_f B_1$ represents the equivalent operator of lossy MZI, considering photon loss in the b -mode. By further utilizing the transformation relation of U_{MZI} (substituting the transformation relation of $U(\phi)$ as well as Eqs. (1)-(2) and (7)), we can derive

$$\begin{aligned} \Pi_b^{loss} &= \frac{\pi}{2} {}_f \langle 0 | \begin{smallmatrix} \vdots \\ \bullet \\ \vdots \end{smallmatrix} \delta \{x_1 a + x_2 b + x_3 b_f\} \\ &\quad \times \delta \{x_1^* a^\dagger + x_2^* b^\dagger + x_3^* b_f^\dagger\} \begin{smallmatrix} \vdots \\ \bullet \\ \vdots \end{smallmatrix} | 0 \rangle_f, \end{aligned} \quad (A3)$$

where

$$\begin{aligned} x_1 &= \frac{i}{2} \left(1 - e^{i\phi} \sqrt{1-l} \right), \\ x_2 &= \frac{1}{2} \left(1 + e^{i\phi} \sqrt{1-l} \right), \\ x_3 &= e^{i\phi} \sqrt{\frac{l}{2}}. \end{aligned} \quad (\text{A4})$$

By using the normal ordering form of the associated Wigner operator, i.e.,

$$\begin{aligned} \Delta_a(\alpha) &= \frac{1}{\pi} : \exp \left[-2(a - \alpha)(a^\dagger - \alpha^*) \right] :, \\ \Delta_b(\beta) &= \frac{1}{\pi} : \exp \left[-2(b - \beta)(b^\dagger - \beta^*) \right] :, \\ \Delta_{b_f}(\gamma_f) &= \frac{1}{\pi} : \exp \left[-2(b_f - \gamma_f)(b_f^\dagger - \gamma_f^*) \right] :, \end{aligned} \quad (\text{A5})$$

the classical correspondence of the Weyl ordering operator can be obtained as follows [63]

$$\begin{aligned} &: f(a, a^\dagger, b, b^\dagger, b_f, b_f^\dagger) : \\ &= 8 \int d^2\alpha d^2\beta d^2\gamma_f f(\alpha, \alpha^*, \beta, \beta^*, \gamma_f, \gamma_f^*) \\ &\quad \times \Delta_a(\alpha) \Delta_b(\beta) \Delta_{b_f}(\gamma_f), \end{aligned} \quad (\text{A6})$$

and by combining the integration within an ordered product (IWOP) technique with the following integral

formula

$$\int \frac{d^2z}{\pi} e^{\zeta|z|^2 + \xi z + \eta z^* + f z^2 + g z^{*2}} = \frac{e^{\frac{-\zeta\xi\eta + \xi^2g + \eta^2f}{\zeta^2 - 4fg}}}{\sqrt{\zeta^2 - 4fg}}, \quad (\text{A7})$$

one can further compute to obtain the normal ordering form of Π_b^{loss} as follows

$$\Pi_b^{loss} = : \exp \left[X_1 a^\dagger a + X_2 b^\dagger b + X_3 a^\dagger b + X_3^* a b^\dagger \right] :, \quad (\text{A8})$$

where

$$\begin{aligned} X_1 &= \frac{l-2}{2} + \sqrt{1-l} \cos \phi, \\ X_2 &= \frac{l-2}{2} - \sqrt{1-l} \cos \phi, \\ X_3 &= \frac{il}{2} - \sqrt{1-l} \sin \phi. \end{aligned} \quad (\text{A9})$$

To facilitate the use of the normal ordering of the parity operator Π_b^{loss} and compute its average value with respect to the input state, we employ the coherent state

representation. The input state can be expressed as

$$\begin{aligned} |\psi\rangle_{in} &= |\alpha\rangle_a \otimes |r, m\rangle_b \\ &= \frac{1}{\sqrt{P_m \cosh r}} \frac{\partial^m}{\partial \tau^m} \int \frac{d^2\beta}{\pi} \\ &\quad \times \exp \left[-\frac{|\beta|^2}{2} + \tau \beta^* - \frac{\tanh r}{2} \beta^{*2} \right] \Big|_{\tau=0} |\alpha\rangle_a |\beta\rangle_b, \end{aligned} \quad (\text{A10})$$

where $|\beta\rangle_b$ is a coherent state used to represent the PASVS input on the b -mode. Using Eqs. (A8) and (A10) and referring to Eq. (A7), we can calculate the average value of the parity operator for under photon loss:

$$\begin{aligned} \langle \Pi_b \rangle &= {}_{in} \langle \psi | \Pi_b^{loss} | \psi \rangle_{in} \\ &= \frac{\exp[A_1 \alpha^2]}{P_m \sqrt{\bar{A}} \cosh r} \\ &\quad \times \frac{\partial^{2m}}{\partial t^m \partial \tau^m} \exp \left[\frac{A_2 + A_3 \alpha}{\bar{A}} \right] \Big|_{t=\tau=0}, \end{aligned} \quad (\text{A11})$$

where

$$\begin{aligned} \bar{A} &= 1 - \tanh^2 r (1 + X_2)^2, \\ A_1 &= X_1 + \frac{\tanh^2 r (1 + X_2) |X_3|^2}{\bar{A}} - \frac{\tanh r}{2\bar{A}} (X_3^2 + X_3^{*2}), \\ A_2 &= (1 + X_2) t \tau - \frac{\tanh r}{2} (1 + X_2)^2 (t^2 + \tau^2), \\ A_3 &= X_3^* t + X_3 \tau - \tanh r (1 + X_2) (X_3 t + X_3^* \tau). \end{aligned} \quad (\text{A12})$$

In particular, for $l = 0$, the result of Eq. (A11) represents the average value of the parity operator in the ideal scenario.

APPENDIX B : THE NORMAL ORDERING FOR OPERATOR IDENTITY AND ITS AVERAGE VALUE

This appendix derives the average of n_b^w with respect to $|\Psi\rangle_S$ in order to obtain an expression for the simplicity of calculating the QFI. The normal ordering of n_b^w is obtained via the operator identity:

$$\begin{aligned} n_b^w &= \frac{\partial^w}{\partial x^w} \exp[x b^\dagger b] \Big|_{x=0} \\ &= \frac{\partial^w}{\partial x^w} : \exp[(e^x - 1) b^\dagger b] : \Big|_{x=0}. \end{aligned} \quad (\text{B1})$$

Based on the coherent state representation of $|\psi\rangle_{in}$ (Eq. (A10)) and utilizing the transformation relation for BS1 (Eq. (1)), the form of $|\Psi\rangle_S$ in the coherent state representation is given by

$$\begin{aligned} |\Psi\rangle_S &= \frac{1}{\sqrt{P_m \cosh r}} \frac{\partial^m}{\partial \tau^m} \int \frac{d^2\beta}{\pi} \exp \left[-\frac{|\beta|^2}{2} + \tau \beta^* \right] \\ &\quad \times \exp \left[-\frac{\tanh r}{2} \beta^{*2} \right] \Big|_{\tau=0} |\alpha_1\rangle_a |\beta_1\rangle_b, \end{aligned} \quad (\text{B2})$$

where $\alpha_1 = (\alpha - i\beta)/\sqrt{2}$ and $\beta_1 = (\beta - i\alpha)/\sqrt{2}$. Using Eqs. (B1) and (B2) along with the IWOP technique and the integral formula Eq. (A7), we obtain

$$\langle n_b^w \rangle = D_{m,w} \{E_M\}, \quad (\text{B3})$$

where

$$\begin{aligned} D_{m,w} \{ \cdot \} &= \frac{1}{P_m \cosh r} \frac{\partial^{2m+w}}{\partial t^m \partial \tau^m \partial x^w} \{ \cdot \} \Big|_{t=\tau=x=0}, \\ E_M &= \frac{M_1}{\sqrt{M_0}} \exp \left[\frac{2M_2 t - M_2^2 \tanh r}{2M_0} \right] \\ &\quad \times \exp \left[-\frac{(s+1)^2 t^2 \tanh r}{2M_0} \right], \end{aligned} \quad (\text{B4})$$

and

$$\begin{aligned} M_0 &= 1 - (s+1)^2 \tanh^2 r, \\ M_1 &= \exp \left[s\alpha \left(\alpha + i\tau + \frac{s\alpha \tanh r}{2} \right) \right], \\ M_2 &= -is\alpha + (e^x - s)(\tau - is\alpha \tanh r), \end{aligned} \quad (\text{B5})$$

where $s = \frac{1}{2}(e^x - 1)$.

APPENDIX C : C_Q FOR THE KERR NONLINEAR PHASE SHIFT CASE

In this appendix, we derive C_Q for the Kerr nonlinear phase shift and its specific expression to obtain the QFI F_Q under photon loss condition. To compute C_Q using Eqs. (15)-(17) and (21) according to the method in Refs. [46] and [59], we first obtain the normal ordering form of $(1-l)^{n_b} n_b^q$ by utilizing the operator identity from Eq. (B1) as follows

$$\begin{aligned} (1-l)^{n_b} n_b^q &= \eta^{n_b} n_b^q \\ &= \frac{\partial^q}{\partial x^q} \exp[n_b \ln \eta] \exp[n_b x] \Big|_{x=0} \\ &=: \frac{\partial^q}{\partial x^q} e^{(\eta e^x - 1)b^\dagger b} \Big|_{x=0} :, \end{aligned} \quad (\text{C1})$$

where for simplicity, we set $\eta = 1 - l$. Based on this equation and further utilizing the IWOP technique, the following summation can be computed for the operators $S_{q,p}$ associated with the Hermitian operators $H_{1,2}$ from Eqs. (16) and (17) to obtain the generalized equation about n_b expressed in terms of the partial differential op-

erator $D_{q,p} = \frac{\partial^{q+p}}{\partial x^q \partial y^p} [\cdot] \Big|_{x=y=0}$ as

$$\begin{aligned} S_{q,p} &= \sum_{j=0}^{\infty} \frac{(1-\eta)^j}{j!} j^p b^{\dagger j} \eta^{n_b} n_b^q b^j \\ &= \sum_{j=0}^{\infty} \frac{(1-\eta)^j}{j!} j^p : (b^\dagger b)^j \frac{\partial^q}{\partial x^q} e^{(\eta e^x - 1)b^\dagger b} \Big|_{x=0} : \\ &=: \sum_{j=0}^{\infty} \frac{[(1-\eta)b^\dagger b]^j}{j!} \frac{\partial^{q+p}}{\partial x^q \partial y^p} e^{(\eta e^x - 1)b^\dagger b + yj} \Big|_{x=y=0} : \\ &=: \frac{\partial^{q+p}}{\partial x^q \partial y^p} e^{[\eta e^x + (1-\eta)e^y - 1]b^\dagger b} \Big|_{x=y=0} : \\ &= \frac{\partial^{q+p}}{\partial x^q \partial y^p} [\eta e^x + (1-\eta)e^y]^{n_b} \Big|_{x=y=0}. \end{aligned} \quad (\text{C2})$$

The final step in the above equation employs the operator identity from Eq. (B1) for conversion.

According to Eq. (15), by substituting the Kraus operator for the Kerr nonlinear phase shift case (Eq. (21)) into Eqs. (16) and (17), and using Eq. (C2) one can further compute that

$$\begin{aligned} C_Q &= 4[K_1^2 \langle \Delta^2 n_b^2 \rangle - K_2 \langle n_b^3 \rangle + K_3 \langle n_b^2 \rangle \\ &\quad - K_4 \langle n_b \rangle - K_5 \langle n_b^2 \rangle \langle n_b \rangle - K_6 \langle n_b \rangle^2], \end{aligned} \quad (\text{C3})$$

where

$$\begin{aligned} K_1 &= \omega_1 \eta^2 - 2\omega_2 \eta - \mu_2, \\ K_2 &= 2\eta [3\omega_1^2 \eta^3 - 3\omega_2^2 \eta^2 - \omega_4 \eta + \omega_5], \\ K_3 &= \eta [11\omega_1^2 \eta^3 - 2\omega_6^2 \eta^2 + \omega_7 \eta - 4\omega_1 \omega_2], \\ K_4 &= \eta \omega_1^2 (6\eta^3 - 12\eta^2 + 7\eta - 1), \\ K_5 &= 2(1-\eta) \eta \omega_1 K_1, \\ K_6 &= (1-\eta)^2 \eta^2 \omega_1^2, \end{aligned} \quad (\text{C4})$$

and

$$\begin{aligned} \omega_1 &= 1 + 2\mu_1 - \mu_2, \\ \omega_2 &= \mu_1 - \mu_2, \\ \omega_3 &= 1 + 2(3\mu_1 - 2\mu_2) + (2\mu_1 - \mu_2)(4\mu_1 - 3\mu_2), \\ \omega_4 &= 7\mu_2 - 6\mu_1 + 24\mu_1 \mu_2 - 14\mu_1^2 - 9\mu_2^2, \\ \omega_5 &= \mu_2 \omega_1 - 2\omega_2^2, \\ \omega_6 &= 9 + 40\mu_1 - 22\mu_2 + 44\mu_1^2 - 48\mu_1 \mu_2 + 13\mu_2^2, \\ \omega_7 &= 7 + 40\mu_1 - 26\mu_2 + 52\mu_1^2 - 64\mu_1 \mu_2 + 19\mu_2^2, \end{aligned} \quad (\text{C5})$$

where parameters μ_1 and μ_2 are optimizable to describe the photon losses occurring before and after the phase shifter. In particular, $\mu_1 = \mu_2 = 0$ or -1 represents photon losses occurring before or after the phase shifter, respectively. Using Eqs. (C3)-(C5), optimizing through $\partial C_Q / \partial \mu_1 = \partial C_Q / \partial \mu_2 = 0$ to find the minimum value of C_Q gives

$$\mu_{1opt} = \frac{G_2 G_5 - G_3 G_4}{G_1 G_4 - 2\eta G_2^2}, \quad (\text{C6})$$

$$\mu_{2opt} = \frac{G_1 G_5 - 2\eta G_2 G_3}{G_1 G_4 - 2\eta G_2^2}, \quad (\text{C7})$$

where

$$G_1 = 2 \left[- (1 - \eta) \eta \left(\langle \Delta^2 n_b^2 \rangle + 2 \langle n_b^2 \rangle \langle n_b \rangle - \langle n_b \rangle^2 \right) - (6\eta^2 - 6\eta + 1) (\langle n_b^3 \rangle + \langle n_b \rangle) + (11\eta^2 - 11\eta + 2) \langle n_b^2 \rangle \right], \quad (\text{C8})$$

$$G_2 = (1 - \eta)^2 \langle \Delta^2 n_b^2 \rangle + 3(1 - \eta)(2\eta - 1) \langle n_b^3 \rangle + (11\eta^2 - 13\eta + 3) \langle n_b^2 \rangle - (6\eta^2 - 6\eta + 1) \langle n_b \rangle - (1 - \eta)(2\eta - 1) \langle n_b^2 \rangle \langle n_b \rangle + \eta(1 - \eta) \langle n_b \rangle^2, \quad (\text{C9})$$

$$G_3 = \eta^2 \langle \Delta^2 n_b^2 \rangle - 3\eta(2\eta - 1) \langle n_b^3 \rangle + (11\eta^2 - 9\eta + 1) \langle n_b^2 \rangle - (6\eta^2 - 6\eta + 1) \langle n_b \rangle + \eta(2\eta - 1) \langle n_b^2 \rangle \langle n_b \rangle + \eta(1 - \eta) \langle n_b \rangle^2, \quad (\text{C10})$$

$$G_4 = - (1 - \eta)^3 \langle \Delta^2 n_b^2 \rangle - 6\eta(1 - \eta)^2 \langle n_b^3 \rangle - \eta(1 - \eta)(11\eta - 4) \langle n_b^2 \rangle - \eta(6\eta^2 - 6\eta + 1) \langle n_b \rangle + 2\eta(1 - \eta)^2 \langle n_b^2 \rangle \langle n_b \rangle + \eta^2(1 - \eta) \langle n_b \rangle^2, \quad (\text{C11})$$

$$G_5 = \eta \left[-\eta(1 - \eta) (\langle \Delta^2 n_b^2 \rangle - \langle n_b \rangle^2) - (6\eta^2 - 6\eta + 1) (\langle n_b^3 \rangle + \langle n_b \rangle) + (11\eta^2 - 11\eta + 2) \langle n_b^2 \rangle + (2\eta^2 - 2\eta + 1) \langle n_b^2 \rangle \langle n_b \rangle \right], \quad (\text{C12})$$

and substituting these into Eq. (C3), along with using Eq. (B3) for $w = 1, 2, 3, 4$, results in $F_Q = C_Q \min$.

-
- [1] H. Vahlbruch, D. Wilken, M. Mehmet, and B. Willke, Laser Power Stabilization beyond the Shot Noise Limit Using Squeezed Light, *Phys. Rev. Lett.* **121**, 173601 (2018).
 - [2] M. Tsang, Quantum limits to optical point-source localization, *Optica* **2**, 646-653 (2015).
 - [3] F. Dolde, H. Fedder, M. W. Doherty, T. Noebauer, F. Rempp, G. Balasubramanian, T. Wolf, F. Reinhard, L. C. L. Hollenberg, F. Jelezko, and J. Wrachtrup, Electric-field sensing using single diamond spins, *Nat. Phys.* **7**, 459 (2011).
 - [4] H. Muntinga *et al.*, Interferometry with Bose-Einstein condensates in microgravity, *Phys. Rev. Lett.* **110**, 093602 (2013).
 - [5] Y. Zhai, Z. Yue, L. Li, and Y. Liu, Progress and applications of quantum precision measurement based on SERF effect, *Front. Phys.* **10**, 969129 (2022).
 - [6] Y. Wu, J. Guo, X. Feng, L. Q. Chen, C. H. Yuan, and W. Zhang, Atom-Light Hybrid Quantum Gyroscope, *Phys. Rev. Applied* **14**, 064023 (2020).
 - [7] Ya. M. Blanter and M. Büttiker, Shot noise in mesoscopic conductors, *Phys. Rep.* **336**, 1 (2000).
 - [8] N. Treps, U. Andersen, B. Buchler, P. K. Lam, A. Maître, H. A. Bachor, and C. Fabre, Surpassing the Standard Quantum Limit for Optical Imaging Using Nonclassical Multimode Light, *Phys. Rev. Lett.* **88**, 203601 (2002).
 - [9] C. M. Caves, Quantum-mechanical noise in an interferometer, *Phys. Rev. D* **23**, 1693 (1981).
 - [10] S. Takeda, T. Mizuta, M. Fuwa, P. v. Loock, and A. Furusawa, Deterministic quantum teleportation of photonic quantum bits by a hybrid technique, *Nature* **500**, 315 (2013).
 - [11] D. Bouwmeester, J. W. Pan, K. Mattle, M. Eibl, H. Weinfurter, and A. Zeilinger, Experimental quantum teleportation, *Nature* **390**, 575 (1997).
 - [12] A. Acín, N. Gisin, and L. Masanes, From Bell's Theorem to Secure Quantum Key Distribution, *Phys. Rev. Lett.* **97**, 120405 (2006).
 - [13] B. Kraus, C. O. Ahonen, M. Möttönen, and J. L. O'Brien, Entanglement-enhanced quantum key distribution, *Phys. Rev. A* **78**, 032314 (2008).
 - [14] L. Y. Hu, M. Al-amri, Z. Y. Liao, and M. S. Zubairy, Continuous-variable quantum key distribution with non-Gaussian operations, *Phys. Rev. A* **102**, 012608 (2020).
 - [15] T. Nagata, R. Okamoto, J. L. O'Brien, K. Sasaki, and S. Takeuchi, Beating the Standard Quantum Limit with Four-Entangled Photons, *Science* **316**, 726 (2007).
 - [16] G. Y. Xiang, B. L. Higgins, D. W. Berry, H. M. Wiseman, and G. J. Pryde, Entanglement-enhanced measurement of a completely unknown optical phase, *Nat. Photonics* **5**, 43 (2011).
 - [17] A. Migliore and A. Messina, Quantum Optics Parity Effect on Generalized NOON States and Its Implications for Quantum Metrology, *Ann. Phys.* **534** 2200304 (2022).
 - [18] J. P. Dowling, Quantum optical metrology – the lowdown on high-NOON states, *Contemp. Phys.* **49**, 125 (2008).
 - [19] J. Joo, W. J. Munro, and T. P. Spiller, Quantum Metrology with Entangled Coherent States, *Phys. Rev. Lett.* **107**, 083601 (2011).
 - [20] B. C. Sanders, Review of entangled coherent states, *J. Phys. A: Math. Theor.* **45**, 244002 (2012).
 - [21] J. Joo, K. Park, H. Jeong, W. J. Munro, K. Nemoto, and T. P. Spiller, Quantum metrology for nonlinear phase shifts with entangled coherent states, *Phys. Rev. A* **86**, 043828 (2012).
 - [22] B. Yurke, S. L. McCall, and J. R. Klauder, SU(2) and SU(1,1) interferometers, *Phys. Rev. A* **33**, 4033 (1986).
 - [23] E. Polino, M. Valeri, N. Spagnolo, and F. Sciarrino, Photonic quantum metrology, *AVS Quantum Sci.* **2**, 024703 (2020).
 - [24] H. Cable and G. A. Durkin, Parameter Estimation with Entangled Photons Produced by Parametric Down-Conversion, *Phys. Rev. Lett.* **105**, 013603 (2010).
 - [25] K. Jiang, C. J. Brignac, Y. Weng, M. B. Kim, H. Lee, and J. P. Dowling, Strategies for choosing path-entangled number states for optimal robust quantum-optical metrology in the presence of loss, *Phys. Rev. A* **86**, 013826 (2012).
 - [26] I. Afek, O. Ambar, and Y. Silberberg, High-NOON States by Mixing Quantum and Classical Light, *Science* **328**, 879 (2010).
 - [27] J. C. F. Matthews, A. Politi, D. Bonneau, and J. L. O'Brien,

- Heralding Two-Photon and Four-Photon Path Entanglement on a Chip, *Phys. Rev. Lett.* **107**, 163602 (2011).
- [28] A. Zavatta, S. Viciani and M. Bellini, Quantum-to-Classical Transition with Single-Photon-Added Coherent States of Light, *Science* **306**, 660 (2004).
- [29] F. Jia, W. Ye, Q. Wang, L. Y. Hu, and H. Y. Fan, Comparison of nonclassical properties resulting from non-Gaussian operations, *Laser Phys. Lett.* **16**, 015201 (2019).
- [30] Q. Q. Kang, Z. K. Zhao, Y. K. Xu, T. Zhao, C. J. Liu, and L. J. Hu, Phase estimation based on multi-photon subtraction operation inside the SU(1,1) interferometer, *Phys. Scripta* **99**, 085111 (2024).
- [31] Y. K. Xu, T. Zhao, Q. Q. Kang, C. J. Liu, L. Y. Hu, and S. Q. Liu, Phase sensitivity of an SU(1,1) interferometer in photon-loss via photon operations, *Opt. Express* **31**, 8414 (2023).
- [32] C. Kumar, Rishabh, M. Sharma, and S. Arora, Parity-detection-based Mach-Zehnder interferometry with coherent and non-Gaussian squeezed vacuum states as inputs, *Phys. Rev. A* **108**, 012605 (2023).
- [33] Y. Ouyang, S. Wang, and L. J. Zhang, Quantum optical interferometry via the photon-added two-mode squeezed vacuum states, *J. Opt. Soc. Am. B* **33**, 001373 (2016).
- [34] R. Birrittella and C. C. Gerry, Quantum optical interferometry via the mixing of coherent and photon-subtracted squeezed vacuum states of light, *J. Opt. Soc. Am. B* **31**, 030586 (2014).
- [35] C. Kumar, Rishabh, and S. Arora, Realistic non-Gaussian-operation scheme in parity-detection-based Mach-Zehnder quantum interferometry, *Phys. Rev. A* **105**, 052437 (2022).
- [36] Z. K. Zhao, Q. Q. Kang, H. Zhang, T. Zhao, C. J. Liu, and L. Y. Hu, Phase estimation via coherent and photon-catalyzed squeezed vacuum states, *Opt. Express* **32**, 28267 (2024).
- [37] H. Zhang, W. Ye, C. P. Wei, Y. Xia, S. K. Chang, Z. Y. Liao, and L. Y. Hu, Improved phase sensitivity in quantum optical interferometer based on multi-photon catalytic two-mode squeezed vacuum states, *Phys. Rev. A* **103**, 013705 (2021).
- [38] S. Wang, X. X. Xu, Y. J. Xu, and L. J. Zhang, Quantum interferometry via a coherent state mixed with a photon-added squeezed vacuum state, *Opt. Commun.* **444**, 102-110 (2019).
- [39] S. Boixo, A. Datta, S. T. Flammia, A. Shaji, E. Bagan, and C. M. Caves, Quantum-limited metrology with product states, *Phys. Rev. A* **77**, 012317 (2008).
- [40] S. Boixo, A. Datta, M. J. Davis, S. T. Flammia, A. Shaji, and C. M. Caves, Quantum Metrology: Dynamics versus Entanglement, *Phys. Rev. Lett.* **101**, 040403 (2008).
- [41] C. P. Wei and Z. M. Zhang, Improving the phase sensitivity of a Mach-Zehnder interferometer via a nonlinear phase shifter, *J. Mod. Opt.* **64**, 743 (2017).
- [42] J. D. Zhang and S. Wang, Nonlinear phase estimation based on nonlinear interferometers with coherent and squeezed vacuum light, *Phys. Lett. A*, **502**, 129400 (2024).
- [43] G. F. Jiao, K. Y. Zhang, L. Q. Chen, W. P. Zhang, and C. H. Yuan, Nonlinear phase estimation enhanced by an actively correlated Mach-Zehnder interferometer, *Phys. Rev. A* **102**, 033520 (2020).
- [44] S. K. Chang, C. P. Wei, H. Zhang, Y. Xia, W. Ye, and L. Y. Hu, Enhanced phase sensitivity with a nonconventional interferometer and nonlinear phase shifter, *Phys. Lett. A*, **384**, 126755 (2020).
- [45] Y. F. Guo, W. Zhong, L. Zhou, and Y. B. Sheng, Supersensitivity of Kerr phase estimation with two-mode squeezed vacuum states, *Phys. Rev. A* **105**, 032609 (2022).
- [46] S. K. Chang, W. Ye, H. Zhang, L. Y. Hu, J. H. Huang, and S. Q. Liu, Improvement of phase sensitivity in an SU(1,1) interferometer via a phase shift induced by a Kerr medium, *Phys. Rev. A* **105**, 033704 (2022).
- [47] J. D. Zhang, Z. J. Zhang, L. Z. Cen, J. Y. Hu, and Y. Zhao, Nonlinear phase estimation: Parity measurement approaches the quantum Cramér-Rao bound for coherent states, *Phys. Rev. A* **99**, 022106 (2019).
- [48] K. P. Seshadreesan, P. M. Anisimov, H. Lee, and J. P. Dowling, Parity detection achieves the Heisenberg limit in interferometry with coherent mixed with squeezed vacuum light, *New J. Phys.* **13**, 083026 (2011).
- [49] K. P. Seshadreesan, S. Kim, J. P. Dowling, and H. Lee, Phase estimation at the quantum Cramér-Rao bound via parity detection, *Phys. Rev. A* **87**, 043833 (2013).
- [50] C. C. Gerry and J. Mimih, The parity operator in quantum optical metrology, *Contemp. Phys.* **51**, 497 (2010).
- [51] W. N. Plick, P. M. Anisimov, J. P. Dowling, H. Lee, and G. S. Agarwall, Parity detection in quantum optical metrology without number-resolving detectors, *New J. Phys.* **12**, 113025 (2010).
- [52] L. Cohen, D. Istrati, L. Dovrat, and H. S. Eisenberg, Super-resolved phase measurements at the shot noise limit by parity measurement, *Opt. Express* **22**, 11945 (2014).
- [53] L. Pezzé and A. Smerzi, Mach-Zehnder Interferometry at the Heisenberg Limit with Coherent and Squeezed-Vacuum Light, *Phys. Rev. Lett.* **100**, 073601 (2008).
- [54] M. D. Lang and C. M. Caves, Optimal Quantum-Enhanced Interferometry Using a Laser Power Source, *Phys. Rev. Lett.* **111**, 173601 (2013).
- [55] S. L. Braunstein and C. M. Caves, Statistical distance and the geometry of quantum states, *Phys. Rev. Lett.* **72**, 3439 (2013).
- [56] S. L. Luo, Wigner-Yanase Skew Information and Uncertainty Relations, *Phys. Rev. Lett.* **91**, 180403 (2003).
- [57] Z. Y. Ou, Complementarity and Fundamental Limit in Precision Phase Measurement, *Phys. Rev. Lett.* **77**, 2352 (1996).
- [58] J. Liu, X. X. Jing, W. Zhong, and X. G. Wang, Quantum Fisher information for density matrices with arbitrary ranks, *Commun. Theor. Phys.* **61**, 45 (2014).
- [59] B. M. Escher, R. L. de Matos Filho, and L. Davidovich, General framework for estimating the ultimate precision limit in noisy quantum-enhanced metrology, *Nat. Phys.* **7**, 406 (2011).
- [60] Z. K. Zhao, H. Zhang, Y. B. Huang, and L. Y. Hu, Phase estimation of a Mach-Zehnder interferometer via the Laguerre excitation squeezed state, *Opt. Express* **31**, 17645 (2023).
- [61] L. Y. Hu and H. Y. Fan, Entangled state for constructing a generalized phase-space representation and its statistical behavior, *Phys. Rev. A* **80**, 022115 (2009).
- [62] H. Y. Fan, Newton-Leibniz integration for ket-bra operators in quantum mechanics (V)—Deriving normally ordered bivariate-normal-distribution form of density operators and developing their phase space formalism, *Ann. Phys. (NY)* **323**, 1502 (2008).
- [63] H. Y. Fan and H. R. Zaidi, Application of IWOP technique to the generalized Weyl correspondence, *Phys. Lett. A* **124**, 303 (1987).